INSTITUTE OF PHYSICS PUBLISHING JOURNAL OF PHYSICS: CONDENSED MATTER

J. Phys.: Condens. Matter **18** (2006) 8383–8394 doi:10.1088/0953-8984/18/35/022

Physical properties of the icosahedral quasicrystal $Al_{60}Cr_{19.9}Fe_{0.1}Ge_{20}$

Zbigniew M Stadnik and Pu Wang

Department of Physics, University of Ottawa, Ottawa, ON, K1N 6N5, Canada

Received 20 June 2006, in final form 3 August 2006
Published 18 August 2006
Online at stacks.iop.org/JPhysCM/18/8383

Abstract

The results of x-ray diffraction, ^{57}Fe Mössbauer spectroscopy, magnetic susceptibility, and electrical conductivity studies of the metastable icosahedral alloy $Al_{60}Cr_{19.9}Fe_{0.1}Ge_{20}$ are reported. The observed broadening of the diffraction Bragg peaks reflects the presence of the topological/chemical disorder. The distribution of the electric quadrupole splitting derived from Mössbauer spectra indicates the existence of a multiplicity of Fe sites. The average quadrupole splitting decreases with temperature as $T^{3/2}$. The vibrations of the Fe atoms are well described by a Debye model, with the Debye temperature of 463(15) K. The temperature dependence of the magnetic susceptibility follows the Curie–Weiss law with the effective magnetic moment of 0.312(3) μ_B per Cr/Fe atom. The origin of the presence of the magnetic moment, and its absence in similar crystalline alloys, is discussed. The temperature dependence of the electrical conductivity can be successfully fitted with the use of theories of quantum interference effects, and values for spin–orbit and inelastic scattering times are extracted from the fits. The scattering process in the studied quasicrystal is dominated by inelastic electron–electron scattering.

(Some figures in this article are in colour only in the electronic version)

1. Introduction

Solids are traditionally divided into two categories: crystalline and amorphous. The dramatic discovery of an icosahedral (i) Al–Mn alloy by Shechtman *et al* [1] extended this dichotomous division by introducing the notion of quasicrystals (QCs). These are materials that possess a new type of long-range translational order, *quasiperiodicity*, and a noncrystallographic orientational order associated with the classically forbidden fivefold, eightfold, tenfold, and twelvefold symmetry axes [2].

Soon after the discovery of the first i QCs in the binary Al–TM (TM = transition metal) system, it was found that the addition of a metalloid (Me) improves their structural quality [3]. These ternary Al–TM–Me i alloys were mainly studied with respect to their formation and

structural properties [4–6]. The only physical property investigated was the electrical resistivity, ρ. It was found that in the i alloys Al–Mn–Ge [4, 7], Al–Mn–Si [8, 9], and Al–Cr–Ge [4, 7], ρ exhibits a nonmetallic behaviour (i.e., $\partial\rho/\partial T$ is negative). For the Al–Cr–Si i alloys, contradictory findings were reported: Inoue *et al* [4] reported that ρ is of metallic type ($\partial\rho/\partial T$ is positive) whereas Kimura *et al* [7] found that ρ is of nonmetallic type. The unexpected increase of ρ with decreasing temperature was interpreted qualitatively in terms of the electron–electron interaction and weak localization effects [8, 9].

In this paper, we report on structural, Mössbauer spectroscopy (MS), magnetic, and transport studies of the i alloy $Al_{60}Cr_{19.9}Fe_{0.1}Ge_{20}$.

2. Experimental procedure

An ingot of composition $Al_{60}Cr_{19.9}Fe_{0.1}Ge_{20}$ was prepared by arc melting in an argon atmosphere a mixture of high-purity Al, Ge, Cr, and Fe enriched to 95% in an ^{57}Fe isotope. The ingot was melt spun in air by ejecting molten alloy at 1423(10) K through a 0.7 mm orifice in a quartz tube onto a surface of a copper wheel rotating with a tangential velocity of 71(1) m s^{-1}. The resulting ribbons were about 2 cm long and 2 mm wide.

X-ray diffraction (XRD) measurements were performed at 298 K in Bragg–Brentano geometry on the PANanalytical X'Pert scanning diffractometer using Cu Kα radiation. The Kβ line was eliminated by using a Kevex PSi2 Peltier-cooled solid-state Si detector. In order to avoid the deviation from intensity linearity of the solid-state Si detector, its parameters and the parameters of the diffractometer were chosen in such a way as to limit the count rate from the most intense Bragg peaks to less than 9000 counts s^{-1} [10]. To allow for the possible instrumental aberration and specimen displacement, corrections were made to the 2θ angles using a fourth-order polynomial calibration curve [11] obtained from the scan of the specimen mixed with 10 wt% of a Si standard [12].

The ^{57}Fe Mössbauer spectroscopy (MS) measurements in the temperature range 4.2–299.7 K were conducted using a standard Mössbauer spectrometer operating in a sine mode and a source of ^{57}Co(Rh) at room temperature. The spectrometer was calibrated with a 6.35 μm-thick α-Fe foil (with a surface density of 107 μg ^{57}Fe cm^{-2}) [13], and the spectra were folded. The full linewidth at half maximum of the inner pair of the α-Fe Zeeman pattern was 0.203(3) mm s^{-1} and this value can be regarded as the resolution of the Mössbauer spectrometer. The surface density of the Mössbauer absorber of the i $Al_{60}Cr_{19.9}Fe_{0.1}Ge_{20}$ alloy was 34 μg ^{57}Fe cm^{-2}. This absorber can therefore be regarded as being thin [14]. The electrical resistivity measurement was made with a standard dc four-probe method between 2.0 and 300 K. The magnetic susceptibility was measured with a Quantum Design superconducting quantum interference device magnetometer in a field of 1 kOe between 2.0 and 300 K.

3. Results and discussion

3.1. Structural characterization

The XRD pattern of the studied sample measured in the 2θ range 20°–100° (figure 1) shows the presence of 11 i Bragg peaks, the weaker of which were not observed earlier [4, 5] in the patterns obtained with a scintillation/proportional counter. This increased sensitivity for weak lines is due to the solid-state detector which has a higher counting efficiency (due to the elimination of a monochromator in the diffracted beam) and lower background count rate as compared to more conventional detectors used in combination with a diffracted-beam monochromator [10]. Two weak Bragg peaks due to an unidentified second phase are also

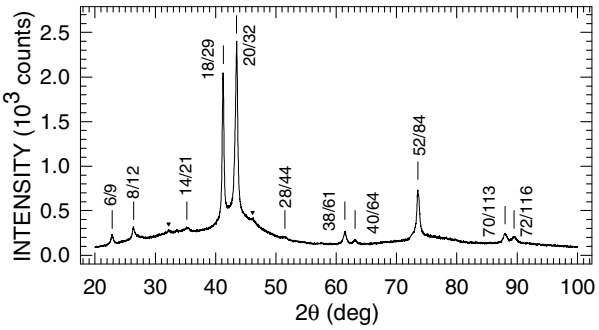

Figure 1. The XRD spectrum of an $Al_{60}Cr_{19.9}Fe_{0.1}Ge_{20}$ alloy at 298 K. The vertical lines labelled with indices N/M above all detected i Bragg peaks correspond to the positions calculated for the Cu Kα_1 radiation, as explained in the text. The position, full width at half maximum, and relative intensity of each detected i peak are given in table 1 together with the corresponding index. The symbol ▼ indicates the peak positions corresponding to an unidentified second phase.

Table 1. Positions in terms of $2\theta_1$ (in degrees) corresponding to Cu Kα_1 radiation and Q_{exp} (in Å^{-1}), full width at half maximum Γ_Q (in Å^{-1}), and relative intensity INT normalized to 100.0 of all detected icosahedral Bragg peaks. Q_{cal} (in Å^{-1}) is the calculated Q value by taking the position of the fourth line with the $I1$ index 18/29 as the reference line. $I1$ and $I2$ are the indices (N/M) and $(h/h', k/k', l/l')$ based on the indexing scheme of Cahn *et al* [17], whereas $I3$ and $I4$ are the indices corresponding, respectively, to the indexing schemes of Elser [18] and Bancel *et al* [19].

$2\theta_1$	Q_{exp}	Q_{cal}	Γ_Q	INT	$I1$	$I2$	$I3$	$I4$
22.813	1.613	1.615	0.032	5.7	6/9	011200	111000	110001
26.343	1.859	1.865	0.024	5.5	8/12	002200	111100	1110$\bar{1}$0
35.276	2.472	2.467	0.018	0.9	14/21	102300	211100	2100$\bar{1}$1
41.198	2.870	2.870	0.019	89.5	18/29	122300	211111	100000
43.415	3.017	3.018	0.028	100.0	20/32	002400	221001	110000
51.449	3.540	3.547	0.016	0.8	28/44	222400	311111	210001
61.389	4.164	4.164	0.039	6.7	38/61	233400	322101	111000
63.058	4.266	4.267	0.046	2.3	40/64	242400	322111	111100
73.529	4.882	4.882	0.024	24.9	52/84	004600	332002	101000
87.989	5.666	5.663	0.031	8.2	70/113	124700	432112	110010
89.411	5.738	5.740	0.044	3.7	72/116	244600	433101	200000

observed (figure 1). The positions of all the detected i Bragg peaks corresponding to Cu Kα_1 radiation (the value of its wavelength λ is 1.540 5981 Å [15]) in terms of the angle $2\theta_1$ and the corresponding wavenumber $Q_{exp} = 4\pi \sin\theta_1/\lambda$, as well as their relative intensities and full widths at half maximum Γ_Q, were determined from the profile fitting using the procedure described by Schreiner and Jenkins [16]. These parameters corresponding to 11 detected i peaks, whose positions are indicated by vertical lines in figure 1, are presented in table 1. This table also contains the theoretical positions Q_{cal} which were calculated by taking the position of the second most intense i peak as the reference. Since there are several schemes employed to index the i peaks, we present in table 1 the indices that correspond to the most frequently used schemes [17–19].

There is a good agreement between the observed Q_{exp} and the theoretical Q_{cal} positions of the i Bragg peaks (figure 1 and table 1). The absence of Bragg peaks that correspond to half-integer indices confirm that the i $Al_{60}Cr_{19.9}Fe_{0.1}Ge_{20}$ QC has a simple icosahedral (SI) six-dimensional Bravais lattice characteristic for i alloys that cannot be produced as

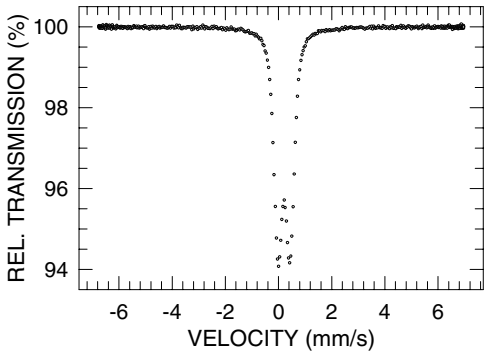

Figure 2. The ^{57}Fe Mössbauer spectrum of the icosahedral $Al_{60}Cr_{19.9}Fe_{0.1}Ge_{20}$ at 299.7 K. The zero-velocity scale is relative to α-Fe at room temperature.

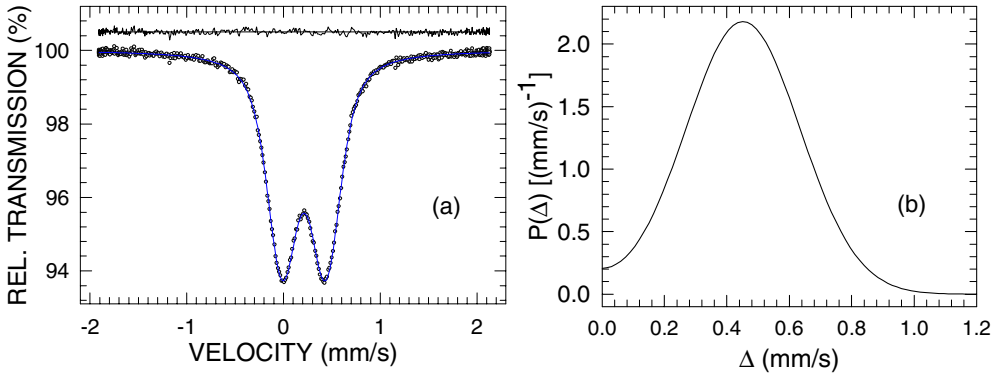

Figure 3. The ^{57}Fe Mössbauer spectrum (a) of the icosahedral $Al_{60}Cr_{19.9}Fe_{0.1}Ge_{20}$ at 297.4 K fitted (solid line) with the distribution $P(\Delta)$ shown in (b). The zero-velocity scale is relative to α-Fe at room temperature. The residuals are shown above the spectrum.

thermodynamically stable. The value of the six-dimensional hypercubic lattice constant calculated from the value Q_{exp} that corresponds to the (18, 29) i peak is 6.558(2) Å. The widths Γ_Q of the i peaks is significantly larger than the instrumental resolution (about 0.006 Å^{-1}) of the XRD spectrometer. This broadening, as well as the small shifts of Q_{exp} from their ideal positions Q_{cal}, indicates the presence of some structural disorder in the i $Al_{60}Cr_{19.9}Fe_{0.1}Ge_{20}$ QC.

A Mössbauer spectrum of the i $Al_{60}Cr_{19.9}Fe_{0.1}Ge_{20}$ QC (figure 2) measured in a wide velocity range shows a pattern due to the presence of only the electric quadrupole interaction; no patterns due to the presence of magnetically ordered Fe-containing second phases are detected.

3.2. Mössbauer spectroscopy

The Mössbauer spectrum of the i $Al_{60}Cr_{19.9}Fe_{0.1}Ge_{20}$ QC consists of a broadened doublet (figure 3(a)) which results from the distribution of the quadrupole splittings, $P(\Delta)$ [20]. A quadrupole splitting

$$\Delta = \tfrac{1}{2} eQ|V_{zz}|(1 + \tfrac{1}{3}\eta^2)^{1/2}, \tag{1}$$

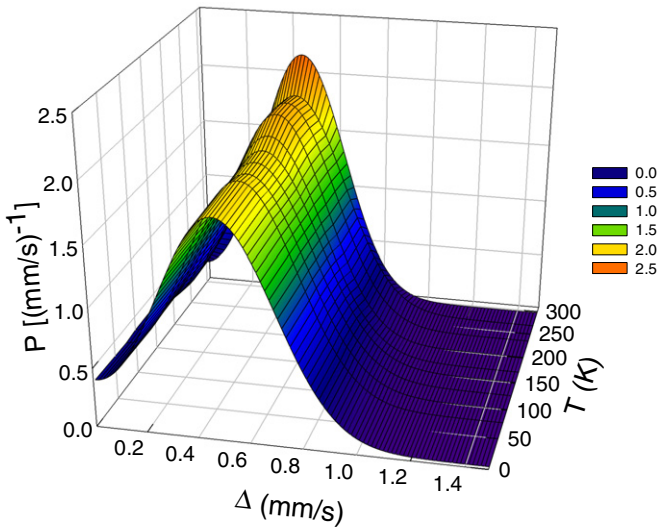

Figure 4. A 3D projection of the distributions $P(\Delta)$ for the icosahedral $Al_{60}Cr_{19.9}Fe_{0.1}Ge_{20}$.

where e is the proton charge and Q is the electric quadrupole moment of the ^{57}Fe nucleus. The asymmetry parameter $\eta = (V_{xx} - V_{yy})/V_{zz}$, $(0 \leqslant \eta \leqslant 1)$, where V_{yy}, V_{xx}, and V_{zz} are the eigenvalues of the electric field gradient (EFG) tensor in order of increasing magnitude [14]. The distribution $P(\Delta)$ is the consequence of the distributions of the EFG and of the asymmetry parameter. The Mössbauer spectrum in figure 3(a) was fitted with the constrained version [21] of the Hesse–Rübartsch method [22]. A slight asymmetry of the spectrum was accounted for by assuming a linear relation between the centre shift, δ, and the quadrupole splitting Δ of the elemental Lorentzian doublets of full width at half maximum Γ, $\delta = \delta_0 + a\Delta$, where δ_0 and a are fitted parameters [20]. The best fit of the Mössbauer spectrum of the i $Al_{60}Cr_{19.9}Fe_{0.1}Ge_{20}$ QC (figure 3(a)) could be obtained with the probability function $P(\Delta)$ shown in figure 3(b). The elemental doublet parameters obtained from the fit are $\Gamma = 0.216(7)$ mm s^{-1}, $\delta_0 = 0.212(2)$ mm s^{-1}, and $a = 8.66(1.22) \times 10^{-5}$. The average values of δ and Δ over the distribution $P(\Delta)$ are $\bar{\delta} = 0.212(2)$ mm s^{-1} and $\bar{\Delta} = 0.452(1)$ mm s^{-1}.

The presence of a wide distribution $P(\Delta)$ observed here (figure 3(b)) and in other i QCs [20] is direct evidence for the multiplicity of Fe sites. In other words, $P(\Delta)$ is a signature of an intrinsic topological disorder present in the i QC. The lack of *ab initio* calculations of the distribution of the EFG in i QCs inhibits a comparison of the experimentally determined $P(\Delta)$ with theory. Such calculations are very desirable since the experimentally determined shape of $P(\Delta)$ could be directly used to determine which of the proposed structural models of a given i QC is the most appropriate.

Distributions $P(\Delta)$ similar to that in figure 3(b) were determined from the fits of the Mössbauer spectra of the i $Al_{60}Cr_{19.9}Fe_{0.1}Ge_{20}$ QC measured at other temperatures (figure 4). One can note a small increase of $\bar{\Delta}$ with decreasing temperature. The temperature dependence of $\bar{\Delta}$ could be fitted (figure 5) to the empirical equation

$$\bar{\Delta}(T) = \bar{\Delta}(0)(1 - BT^{3/2}), \tag{2}$$

where $\bar{\Delta}(0)$ is the value of $\bar{\Delta}$ at 0 K and B is a constant. Such a $T^{3/2}$ temperature dependence has been observed in many metallic noncubic crystalline alloys [23], in some amorphous [24, 25] alloys, and recently in QCs [25, 26] over temperature ranges from a few

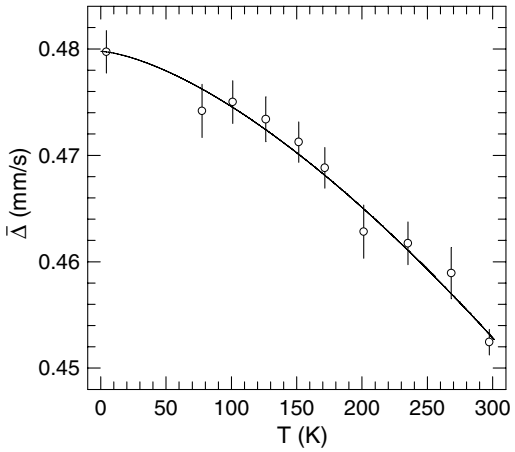

Figure 5. The temperature dependence of the average quadrupole splitting of the icosahedral $Al_{60}Cr_{19.9}Fe_{0.1}Ge_{20}$. The solid line is the fit to equation (2), as explained in the text.

K to the melting point. This seemingly universal $T^{3/2}$ dependence is not well understood. Its origin seems to be associated with a strong temperature dependence of mean-square lattice displacements and, to a lesser extent, with the temperature dependence of lattice expansion [27]. The values of $\bar{\Delta}(0)$, B determined from the fit for the i $Al_{60}Cr_{19.9}Fe_{0.1}Ge_{20}$ QC are 0.480(1) mm s^{-1}, 1.08(5) $\times$ 10^{-5} $K^{-3/2}$. The value of B is similar to that found for other metallic amorphous alloys and QCs [24–26].

The average centre shift at temperature T, $\bar{\delta}(T)$, determined from the fits of the spectra of the studied sample measured at different temperatures is given by

$$\bar{\delta}(T) = \delta_0 + \delta_{SOD}(T), \tag{3}$$

where δ_0 is the intrinsic isomer shift and $\delta_{SOD}(T)$ is the second-order Doppler (SOD) shift which depends on lattice vibrations of the Fe atoms [14]. In terms of the Debye approximation of the lattice vibrations, $\delta_{SOD}(T)$ is expressed [14] by the Debye temperature, Θ_D, as

$$\delta_{SOD}(T) = -\frac{9}{2}\frac{kT}{Mc}\left(\frac{T}{\Theta_D}\right)^3 \int_0^{\Theta_D/T} \frac{x^3\,dx}{e^x - 1}, \tag{4}$$

where M is the mass of the Mössbauer nucleus, k is the Boltzmann constant, and c is the speed of light. By fitting the experimental data $\bar{\delta}(T)$ (figure 6) to equation (3), the quantities δ_0 and Θ_D were found to be, respectively, 0.331(2) mm s^{-1} and 463(15) K. The value of Θ_D found here is comparable to the values of Θ_D found for other i QCs [25, 26].

3.3. Magnetic susceptibility

The magnetic susceptibility of the i $Al_{60}Cr_{19.9}Fe_{0.1}Ge_{20}$ QC measured in an applied magnetic field of 1 kOe between 2.0 and 300 K is shown in figure 7. Between 20 and 300 K, the $\chi(T)$ data can be well fitted to

$$\chi = \chi_0 + \frac{C}{T - \theta_p}, \tag{5}$$

where χ_0 is the temperature-independent magnetic susceptibility, C is the Curie constant, and θ_p is the paramagnetic Curie temperature. The Curie constant can be expressed as $C = \frac{N\mu_{eff}^2}{3k}$, where N is the concentration of magnetic atoms per unit mass and μ_{eff} is the

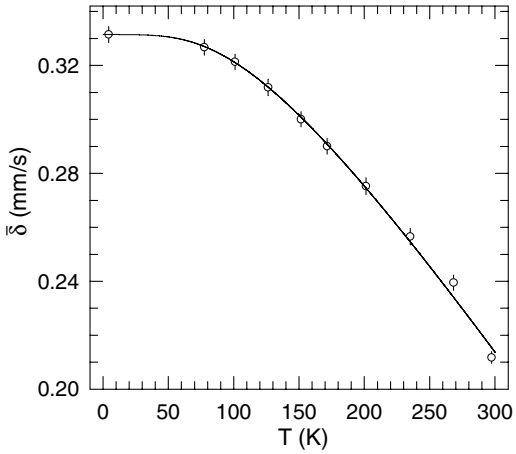

Figure 6. The temperature dependence of the average centre shift of the icosahedral $Al_{60}Cr_{19.9}Fe_{0.1}Ge_{20}$. The solid line is the fit to equation (3), as explained in the text.

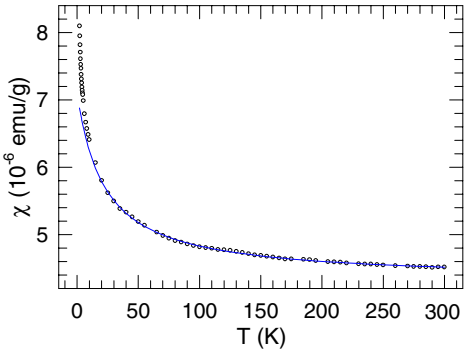

Figure 7. The temperature dependence of the magnetic susceptibility of the icosahedral $Al_{60}Cr_{19.9}Fe_{0.1}Ge_{20}$, measured in a field of kOe. The solid line is the fit to equation (5), as explained in the text.

effective magnetic moment. The values of χ_0, C, and θ_p obtained from the fit are, respectively, $4.33(1) \times 10^{-6}$ emu g^{-1}, $6.15(13) \times 10^{-5}$ emu K g^{-1}, and $-22.1(9)$ K. This value of C corresponds to μ_{eff} of 0.312(3) μ_B per TM atom. Magnetic susceptibility measurements on an i QC of a similar composition $Al_{65}Cr_{20}Ge_{15}$ [28] found $\theta_p = -10.9$ K and $\mu_{eff} = 0.45$ μ_B per Cr atom.

A deviation from the Curie–Weiss law below 20 K (figure 7) may be due to the presence of some magnetic impurity in the sample. The negative values of θ_p indicates the predominantly antiferromagnetic interaction between the TM atoms, which was also observed in other i Al–TM QCs [28, 29]. Magnetic susceptibility measurements in Al–Cr crystalline alloys showed that Cr atoms do not carry a magnetic moment [30]. No measurable magnetic moment on Cr atoms was found in the i $Al_{74}Cr_{20}Si_6$ QC [31]. A sizeable magnetic moment of 0.312(3) μ_B observed here confirms an earlier observation [28] that there is a local magnetic moment on Cr in the i Al–Cr–Ge QC.

The non-zero value of μ_{eff} on the Cr atoms in the i Al–Cr–Ge QCs, and its absence in Al–Cr crystalline alloys, raises the question of its origin. It is conceivable that the i symmetry induces

a large density of states at the Fermi level, $N(E_F)$, and hence leads via the Stoner criterion to the formation of the magnetic moment on the Cr atoms [32]. There are neither electronic structure calculations nor the experimental electronic structure studies for the i Al–Cr–Ge QC available to ascertain the possibility of the high $N(E_F)$. However, one can use the following qualitative argument to show that this value must be small. The formation and stability of the i QCs appears to be qualitatively explained in terms of the Hume-Rothery rules [3]. The i QCs seem to form for certain well defined values of the electron-per-atom ratio e/a [3]. At these critical ratios the Fermi sphere of radius k_F just touches a Brillouin zone plate, i.e., $2k_F = Q$. This corresponds to the opening of an energy gap at the Fermi surface, giving rise to a minimum of $N(E_F)$. Assuming the valence electron numbers of +3 for Al, +4 for Ge, −4.66 for Cr, and −2.66 for Fe [3], one can find that the value of e/a for the i $Al_{60}Cr_{19.9}Fe_{0.1}Ge_{20}$ QC is 1.670. The radius of the Fermi sphere is calculated from the equation $k_F = (3\pi^2 n_e)^{1/3}$, where n_e is the electron concentration. The electron concentration can be derived from the relation $n_e = \frac{(e/a)dN_A}{M}$, where d is the mass density of the alloy, M is its atomic weight, and N_A is the Avogadro number. With the value $e/a = 1.67$, one gets $2k_F = 2.880$ Å^{-1}. The latter compares well with the Q value of 2.870 Å^{-1} corresponding to the 18/29 i peak (table 1). It thus appears that i symmetry, similarly as is the case for the i Al–Mn QCs [33], is not responsible for the formation of a magnetic moment on the Cr atoms.

The most probable origin of the non-zero magnetic moment on the Cr atoms in the i $Al_{60}Cr_{19.9}Fe_{0.1}Ge_{20}$ QC is the presence of the topological disorder inherent to the i structure. This interpretation was first suggested in [34] in relation to the i Al–Mn QCs. It was later justified theoretically [35]. It is well known that magnetic interactions depend crucially upon interatomic distances. In alloys containing TM atoms it was shown using total-energy band calculations [36] that there is a system-dependent critical separation between the TM atoms below which they do not carry a magnetic moment; this moment appears for separations larger than the critical one. This general result then implies that the presence of topological disorder, which involves different TM–TM separations, in an alloy may be crucial for the formation of a magnetic moment. The presence of this disorder in the studied i $Al_{60}Cr_{19.9}Fe_{0.1}Ge_{20}$ QC is clearly manifested in the broadening of the i Bragg peaks and the appearance of the distribution $P(\Delta)$.

3.4. Electrical conductivity

The temperature dependence of ρ and of the electrical conductivity σ ($\sigma = 1/\rho$) for the i $Al_{60}Cr_{19.9}Fe_{0.1}Ge_{20}$ QC is shown in figure 8. The most salient feature of this dependence is a remarkably large value of ρ, as compared to that of amorphous and crystalline alloys of similar composition, and the negative $\partial\rho/\partial T$ over a large temperature range. At low temperatures, ρ increases with temperature from $\rho_{2\,K} = 1398.2$ $\mu\Omega$ cm and passes through a shallow maximum at 37.2 K where $\rho_{37.2\,K} = 1407.6$ $\mu\Omega$ cm; the total increase from 2 to 37.2 K, $(\rho_{37.2\,K} - \rho_{2\,K})/\rho_{37.2\,K} = 0.7\%$, is very small. Above this temperature, ρ decreases almost linearly with increasing temperature to $\rho_{300\,K} = 1345.5$ $\mu\Omega$ cm, thus by 4.4% of its maximum value.

The temperature dependence of σ in QCs was shown to be well described by the quantum interference effects (QIEs), i.e., the electron–electron interaction (EEI) and the weak localization (WL) effects [37]. The form of the temperature dependence of σ due to QIEs is

$$\sigma(T) = \sigma(0) + \Delta\sigma_{EEI}(T) + \Delta\sigma_{WL}(T), \tag{6}$$

where $\sigma(0)$ is the temperature-independent background conductivity, $\Delta\sigma_{EEI}$ is the EEI

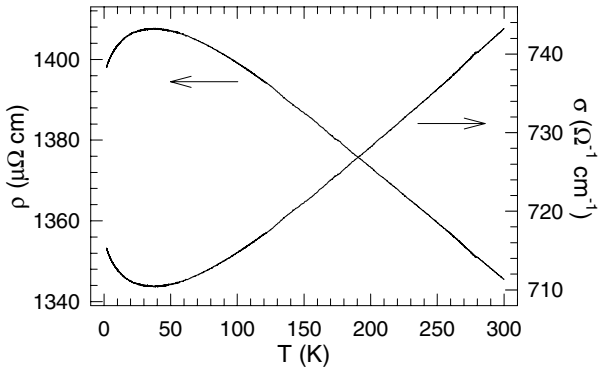

Figure 8. The temperature dependence of the electrical resistivity and conductivity of the icosahedral $Al_{60}Cr_{19.9}Fe_{0.1}Ge_{20}$.

contribution, and $\Delta\sigma_{WL}$ is the WL contribution. The EEI contribution [38] is written as

$$\Delta\sigma_{EEI}(T) = \frac{1.3}{\sqrt{2}}\frac{e^2}{4\pi^2\hbar}\left(\frac{4}{3} - \frac{3}{2}F_\sigma\right)\sqrt{\frac{kT}{\hbar D}}, \tag{7}$$

where F_σ is the Coulomb interaction parameter and D is the diffusion constant. The WL contribution [38] is in the form

$$\Delta\sigma_{WL}(T) = \frac{e^2}{2\pi^2\hbar\sqrt{D}}\left(3\sqrt{\frac{1}{\tau_{so}} + \frac{1}{4\tau_i}} - \sqrt{\frac{1}{4\tau_i}} - 3\sqrt{\frac{1}{\tau_{so}}}\right), \tag{8}$$

where τ_{so} is the spin–orbit scattering time and τ_i is the inelastic scattering time. The last term in equation (8) is added in order to get $\Delta\sigma_{WL} = 0$ at $T = 0$. Only τ_i in equation (8) is temperature dependent and is usually expressed by a simple power law $\tau_i = \tau_{i0}T^{-p}$, where τ_{i0} is a constant and the exponent p depends on the type of inelastic scattering mechanism. Combining equations (7) and (8), the final form of the expression for the conductivity due to QIE corrections is

$$\sigma(T) = \sigma(0) + a\sqrt{T} + b\left(3\sqrt{1 + cT^d} - \sqrt{cT^d} - 3\right), \tag{9}$$

where the fitted parameters $a = \frac{1.3}{\sqrt{2}}\frac{e^2}{4\pi^2\hbar}\left(\frac{4}{3} - \frac{3}{2}F_\sigma\right)\sqrt{\frac{k}{\hbar D}}$, $b = \frac{e^2}{2\pi^2\hbar\sqrt{D\tau_{so}}}$, $c = \frac{\tau_{so}}{4\tau_{i0}}$, and $d = p$.

The value of the diffusivity can be estimated using the Einstein equation for the Boltzmann conductivity $\sigma(0) = e^2N(E_F)D$. The value of $\sigma(0) = 717.3(1)\ \Omega^{-1}\ cm^{-1}$ was obtained from the extrapolation of the experimental $\sigma(T)$ data (figure 8) to 0 K. $N(E_F)$ was estimated from the electronic specific heat coefficient γ of 1.0 mJ ($mol^{-1}\ K^{-2}$) [39] via the relation $\gamma = \pi^2kN(E_F)/3$. This gave $D = 0.175\ cm^2\ s^{-1}$. The electrical conductivity of the i $Al_{60}Cr_{19.9}Fe_{0.1}Ge_{20}$ QC was fitted to equation (9) (figure 9), and from the values of a, b, c, and d one can extract values of F_σ, τ_{so}, τ_{i0}, and p (table 2). It is not obvious up to what maximum temperature, T_{max}, do QIEs contribute to $\sigma(T)$ [37]. It was demonstrated [40] that QIE corrections to $\sigma(T)$ in the i Al–Cu–Fe QCs extend up to $T_{max} = 300$ K. We first fitted the subsection of the $\sigma(T)$ data between 2 K and $T_{max} = 100$ K (figure 9(a)). A good fit was obtained with sensible values [37, 40, 41] for the F_σ, τ_{so}, τ_{i0}, and p parameters (table 2). It can be seen that the fitted curve continues to describe $\sigma(T)$ data well above 100 K up to about 200 K. Next we fitted the subsection of the $\sigma(T)$ data between 2 K and $T_{max} = 200$ K (figure 9(b)). A good fit for slightly different values of F_σ, τ_{so}, τ_{i0}, and p (table 2) is evident.

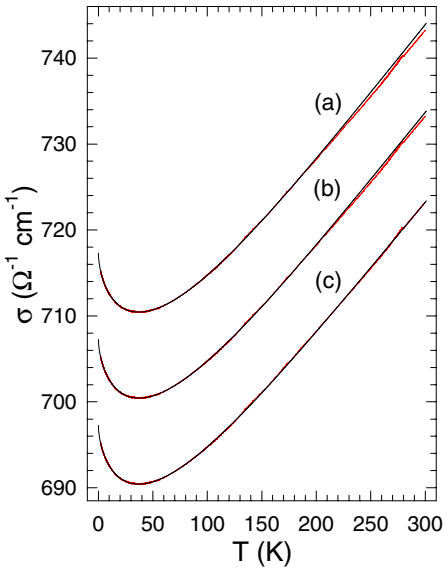

Figure 9. The electrical conductivity (red curve) fitted (solid line) to equation (9) between 2.0 K and (a) $T_{max} = 100$ K, (b) $T_{max} = 200$ K, and (c) $T_{max} = 300$ K, as explained in the text. The experimental and fitted curves in (b) and (c) are shifted by 10 and 20 Ω^{-1} cm^{-1}, respectively.

Table 2. EEI and WL parameters obtained from the fits of $\sigma(T)$ to equation (9) between 2.0 K and T_{max}.

T_{max} (K)	F_σ	τ_{so} (ps)	τ_{i0} (ps)	p
100	0.885(13)	0.521(86)	104(21)	1.27(1)
200	0.902(2)	0.659(23)	128(5)	1.29(4)
300	0.923(2)	0.895(25)	166(5)	1.31(4)

The fitted curve describes $\sigma(T)$ data well above 200 K up to about 220 K. Figure 9(c) shows the fit in the entire temperature range 2–300 K for the F_σ, τ_{so}, τ_{i0}, and p parameters given in table 2.

The Coulomb interaction parameter F_σ found here (table 2) is within the range 0.6–1.5 found for other i QCs [40, 41]. The value of τ_{so} of $\sim$1 ps is of the same order of magnitude as that found in other i QCs [40, 41]. At 300 K, τ_i is of the order 0.1 ps, which is consistent with the corresponding values found in i Al–Cu–Fe QCs [40, 41]. The p value of about 1.3 indicates that the scattering mechanism in the studied QC is dominated by inelastic electron–electron scattering [40]. It is concluded that QIE corrections to σ account well for the temperature dependence of $\sigma(T)$ up to room temperature.

4. Conclusions

A distribution of the electric quadrupole splitting in the studied quasicrystal reflects the presence of a structural disorder. The temperature dependence of the average quadrupole splitting follows the $T^{3/2}$ dependence. The vibrations of the Fe atoms are well described by a Debye model, with the Debye temperature of 463(15) K. The formation of the magnetic moment of 0.312(3) μ_B per Cr/Fe atom results from the topological disorder inherent to the

icosahedral structure. The temperature dependence of the electrical conductivity up to room temperature is well accounted for quantitatively by theories of quantum interference effects. The scattering process in the studied quasicrystal is dominated by inelastic electron–electron scattering.

Acknowledgment

This work was supported by the Natural Sciences and Engineering Research Council of Canada.

References

[1] Shechtman D, Blech I, Gratis D and Cahn J W 1984 *Phys. Rev. Lett.* **53** 1951
[2] Suck J-B, Schreiber M and Häussler P (ed) 2002 *Quasicrystals, An Introduction to Structure, Physical Properties, and Applications* (Berlin: Springer)
[3] Tsai A P 1999 *Physical Properties of Quasicrystals* ed Z M Stadnik (Berlin: Springer) p 5
[4] Inoue A, Kimura H M, Masumoto T, Tsai A P and Bizen Y 1987 *J. Mater. Sci. Lett.* **6** 771
[5] Inoue A, Kimura H M and Masumoto T 1987 *J. Mater. Sci.* **22** 1864
[6] Inoue A, Bizen Y and Masumoto T 1988 *Met. Trans.* A **19** 383
[7] Kimura H M, Inoue A, Bizen Y, Masumoto T and Chen H S 1988 *Mater. Sci. Eng.* **99** 449
[8] Kimura K, Yamane H, Hashimoto T and Takeuchi S 1987 *Mater. Sci. Forum* **22–24** 471
[9] Kimura K, Yamane H, Hashimoto T and Takeuchi S 1988 *Mater. Sci. Eng.* **99** 435
[10] Bish D L and Chipera S J 1989 *Powder Diffr.* **4** 137
[11] Wong-Ng W and Hubbard C R 1987 *Powder Diffr.* **2** 242
[12] 2000 *Standard Reference Material 640c, Silicon Powder Line Position and Line Shape Standard for X-ray Diffraction* Natl. Inst. Stand. Techn. (US)
[13] Cali J P (ed) 1971 *Certificate of Calibration, Iron Foil Mössbauer Standard,* NBS (US) Circular No. 1541 (Washington, DC: US Government Printing Office)
[14] Greenwood N N and Gibb T C 1971 *Mössbauer Spectroscopy* (London: Chapman and Hall)
Gütlich P, Link R and Trautwein A 1978 *Mössbauer Spectroscopy and Transition Metal Chemistry* (Berlin: Springer)
[15] Jenkins R and Schreiner W N 1989 *Powder Diffr.* **4** 74
[16] Schreiner W N and Jenkins R 1983 *Adv. X-ray Anal.* **26** 141
[17] Cahn J W, Shechtman D and Gratias D 1986 *J. Mater. Res.* **1** 13
[18] Elser V 1986 *Acta Crystallogr.* A **42** 36
[19] Bancel P A, Heiney P A, Stephens P W, Goldman A I and Horn P M 1985 *Phys. Rev. Lett.* **54** 2422
[20] Stadnik Z M 1996 *Mössbauer Spectroscopy Applied to Magnetism and Materials Science* vol 2, ed G J Long and F Grandjean (New York: Plenum) p 125
[21] Le Caër G and Dubois J M 1979 *J. Phys. E: Sci. Instrum.* **12** 1083
[22] Hesse J and Rübartsch A 1974 *J. Phys. E: Sci. Instrum.* **7** 526
[23] Kaufmann E N and Vianden R J 1979 *Rev. Mod. Phys.* **51** 161 and references therein
[24] Deppe P and Rosenberg M 1983 *Hyperfine Interact.* **15/16** 735
Kopcewicz M, Kopcewicz B and Gonser U 1987 *J. Magn. Magn. Mater.* **66** 79
Mao M, Ryan D H and Altounian Z 1994 *Hyperfine Interact.* **92** 2163
[25] Stadnik Z M, Saida J and Inoue A 2001 *Ferroelectrics* **250** 297
Stadnik Z M, Rapp Ö, Srinivas V, Saida J and Inoue A 2002 *J. Phys.: Condens. Matter* **14** 6883
[26] Stadnik Z M, Takeuchi T and Mizutani U 2000 *Mater. Sci. Eng.* A **294–296** 331
Brand R A, Voss J and Calvayrac Y 2000 *Mater. Sci. Eng.* A **294–296** 666
Stadnik Z M, Takeuchi T, Tanaka N and Mizutani U 2003 *J. Phys.: Condens. Matter* **15** 6365
Stadnik Z M and Zhang G 2006 *J. Phys.: Condens. Matter* **17** 6599
[27] Jena P 1976 *Phys. Rev. Lett.* **36** 418
Nishiyama K, Dimmling F, Kornrumph Th and Riegel D 1976 *Phys. Rev. Lett.* **37** 357
Christiansen J, Heubes P, Keitel R, Klinger W, Loeffler W, Sandner W and Witthuhn W 1976 *Z. Phys.* B **24** 177
[28] McHenry M E, Dunlap R A, Srinivas V, Bahadur D and O'Handley R C 1990 *Phys. Rev.* B **41** 6933
[29] Stadnik Z M, Stroink G, Ma H and Williams G 1989 *Phys. Rev.* B **39** 9797
[30] Taylor M A 1961 *Proc. Phys. Soc. London* **78** 1244
[31] McHenry M E, Srinivas V, Bahadur D, O'Handley R C, Lloyd D J and Dunlap R A 1989 *Phys. Rev.* B **39** 3611

[32] Stadnik Z M and Müller F 1995 *Phil. Mag.* B **71** 221 and references therein
[33] de Coulon V, Reuse F A and Khanna S N 1993 *Phys. Rev.* B **48** 814
Liu F, Khanna S N, Magaud L, Jena P, de Coulon V, Reuse F, Jaswal S S, He X-G and Cyrot-Lackmann F 1993 *Phys. Rev.* B **48** 1295
[34] Hauser J J, Chen H S, Espinosa G P and Waszczak J V 1986 *Phys. Rev.* B **34** 4674
Warren W W, Chen H-S and Espinosa G P 1986 *Phys. Rev.* B **34** 4902
[35] Bratkovsky A M, Smirnov A V, Nguyen Manh D and Pasturel A 1995 *Phys. Rev.* B **52** 3056
Smirnov A V and Bratkovsky A M 1996 *Phys. Rev.* B **53** 8515
[36] Moruzzi V L and Marcus P M 1992 *Phys. Rev.* B **45** 2934
Moruzzi V L and Marcus P M 1993 *Phys. Rev.* B **47** 7878
[37] Rapp Ö 1999 *Physical Properties of Quasicrystals* ed Z M Stadnik (Berlin: Springer) p 127
[38] Lee P A and Ramakrishnan T V 1985 *Rev. Mod. Phys.* **57** 287
Altshuler B L and Aronov A G 1985 *Electron–Electron Interaction in Disordered Conductors* ed A L Efros and M Pollak (New York: Elsevier) p 1
Dugdale J S 1995 *The Electrical Properties of Disordered Metals* (Cambridge: Cambridge University Press)
[39] Mizutani U 1993 *Mater. Sci. Eng.* B **19** 82
[40] Ahlgren M, Lindqvist P, Rodmar M and Rapp Ö 1997 *Phys. Rev.* B **55** 14847
Rodmar M, Ahlgren M and Rapp Ö 1995 *Proc. 5th Int. Conf. Quasicrystals* ed C Janot and R Mosseri (Singapore: World Scientific) p 518
[41] Chernikov M A, Bernasconi A, Belli C and Ott H R 1993 *Europhys. Lett.* **21** 767
Ahlgren M, Rodmar M, Klein Th and Rapp Ö 1995 *Phys. Rev.* B **51** 7287
Lindqvist P, Lanco P, Berger C, Jansen A G M and Cyrot-Lackmann F 1995 *Phys. Rev.* B **51** 4796